Author's Accepted Manuscript

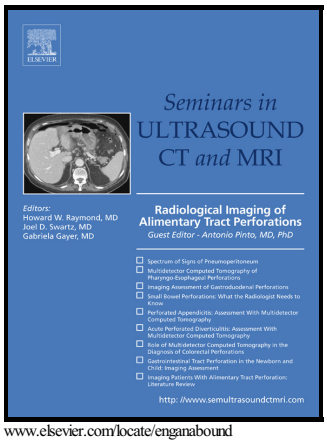

www.elsevier.com/locate/enganabound

Hepatic Steatosis: Etiology, Patterns and Quantification

Ilkay S. Idilman, Ilknur Ozdeniz, Musturay Karcaaltincaba

PII: S0887-2171(16)30065-8
DOI: http://dx.doi.org/10.1053/j.sult.2016.08.003
Reference: YSULT720

To appear in: *Seminars in Ultrasound, CT, and MRI*

Cite this article as: Ilkay S. Idilman, Ilknur Ozdeniz and Musturay Karcaaltincaba, Hepatic Steatosis: Etiology, Patterns and Quantification, *Seminars in Ultrasound, CT, and MRI,* http://dx.doi.org/10.1053/j.sult.2016.08.003

HEPATIC STEATOSIS: ETIOLOGY, PATTERNS AND QUANTIFICATION

[1,2]Ilkay S. Idilman, MD, [1,3]Ilknur Ozdeniz, MD, [1]Musturay Karcaaltincaba MD.

[1]Liver Imaging Team, Hacettepe University, School of Medicine, Department of Radiology, Ankara-Turkey.

[2]Ankara Atatürk Education and Research Hospital, Department of Radiology, Ankara-Turkey

[3]Bursa State Hospital, Department of Radiology, Bursa-Turkey

Address for correspondence

Musturay Karcaaltincaba, M.D.,

Hacettepe University, School of Medicine,

Department of Radiology,

Ankara, Turkey 06100

Phone:+903123051188-427

e-mail: musturayk@yahoo.com

ABSTRACT

Hepatic steatosis can occur due to nonalcoholic fatty liver disease (NAFLD), alcoholism, chemotherapy, metabolic, toxic and infectious causes. Pediatric hepatic steatosis is also becoming more frequent and can have distinctive features. Most common pattern is

diffuse form, however it can present as heterogenous, focal, multinodular, perilesional, perivascular, subcapsular and lobar forms. Focal steatosis and fat sparing can occur due to presence of veins of Sappey, pancreaticoduodenal, aberrant right and left gastric veins, which drain into the liver as third inflow. Hypersteatosis and multinodular forms can mimic metastasis in cancer patients. Perilesional fat can be seen in insulinoma. Recent introduction of proton density fat fraction (PDFF) enabled easy and reproducible quantification of hepatic fat. Follow-up of NAFLD patients can be performed for the assessment of treatment response using PDFF as biomarker. Multiecho gradient echo techniques also simultaneously calculate T2* maps, which is important to rule out coexisting hepatic iron overload. NAFLD can progress into steatohepatitis (NASH), which can end up with cirrhosis. MR elastography and functional evaluation with Gd-EOB-DTPA are becoming important for monitoring this process. Hepatocellular carcinoma can develop in patients with NAFLD, which is usually a large tumor with necrotic center. In the future, fatty acid maps obtained by MR may allow more detailed analysis of steatosis. MR is superior to ultrasonography and CT for comprehensive evaluation of steatosis.

INTRODUCTION

Hepatic steatosis is defined as excessive triglyceride accumulation within the hepatocytes. There are two major conditions associated with hepatic steatosis: nonalcoholic fatty liver disease (NAFLD) and alcoholic fatty liver disease. Besides, variable causes such as metabolic, nutritional, drug induced (chemotherapy and steroids) and hepatitis C virus infection are listed in the pathogenesis of hepatic steatosis (1). The natural course of hepatic steatosis varies according to the etiology and accompanied conditions such as inflammation and fibrosis, which has a potential to progress into cirrhosis and liver failure. Therefore it is

important to diagnose and quantify hepatic steatosis. Liver biopsy is the current gold standard for evaluating a patient with suspected hepatic steatosis. However, there are potential drawbacks of liver biopsy such as sampling error, interpretation variability, cost and associated morbidity (2,3). Hence, imaging modalities are commonly used for this purpose. In this article we will review etiology, imaging patterns and quantification of hepatic steatosis with conventional and advanced imaging techniques.

ETIOLOGY

Nonalcoholic Fatty Liver Disease

NAFLD is the most common form of hepatic steatosis and affects 30%-40% of men and 15%-20% of women in the general population (4). It is accepted as hepatic manifestation of metabolic syndrome and has a strong relationship with insulin resistance, atherosclerosis, obesity, dyslipidemia and hypertension (5,6). Accumulation of lipids in hepatocytes causes oxidative stress and inflammatory response that leads to non-alcoholic steatohepatitis (NASH) that may progress to cirrhosis. It is estimated that NAFLD will become the most common indication for liver transplantation by 2030 (7).

Alcoholic Fatty Liver Disease

Chronic alcohol intake is another cause of hepatic steatosis and up to 90% of the alcoholics have alcoholic fatty liver disease (AFLD) (8). Patients with pure AFLD have a 10% risk of progressing to cirrhosis (9). A consumption of 30 g ethanol/day was shown to increase the risk of chronic liver damage and cirrhosis in alcoholic patients (10). Furthermore, female gender, cigarette smoking, obesity and accompanying hepatic disorders are predisposing factors for liver damage in AFLD (9).

Metabolic Causes

These factors are divided into two main categories: inborn errors of metabolism and acquired metabolic disorders. Inborn errors of metabolism include abetalioproteinemia, galactosemia, glycogen storage disease, hereditary fructose intolerance, homocystinuria, systemic carnitine deficiency, tyrosinemia, Refsum's syndrome, Schwachman syndrome, Weber-Christian syndrome and Wilson disease (1). Acquired metabolic disorders are inflammatory bowel disease, jejunoileal bypass, Kwashiorkor and marasmus, starvation and cachexia and total parenteral nutrition (1).

Viral Causes

Hepatitis C virus (HCV), especially genotype 3 is associated with hepatic steatosis. The prevalence of hepatic steatosis in chronic HCV infection is ranging from 40-80% (11,12). The possible mechanisms of hepatic steatosis in HCV infection are direct steatogenic or insulin resistance effect of HCV viral proteins (13). Direct steatogenic effect explains hepatic steatosis even in the absence of obesity in patients infected with genotype 3a HCV. Beyond, several viral proteins interfere with insulin signaling which results with insulin resistance and hepatic steatosis (13). Hepatic steatosis observed in patients infected with hepatitis B virus (HBV) is thought to be associated with metabolic factors rather than HBV infection.

Drug-induced hepatic steatosis

Hepatic steatosis can be seen as an adverse reaction to some medications such as tetracycline, valproic acid, dexamethasone, amiadarone, methotrexate, tamoxifen, and acetylsalicylic acid (14). Either microvesicular or macrovesicular steatosis can be observed in drug-induced hepatic steatosis (DIHS). The underlying metabolic syndrome and obesity may aggravate the process of DIHS. It generally occurs with therapy lasting several weeks or months and is reversible after discontinuation. However, some medications should be

continued even the detection of DIHS such as chemotherapeutic agents and it is important to monitor the signs of progressive liver damage, which can end up with portal hypertension in these patients (Fig. 1).

Pediatric Hepatic Steatosis

Different factors can be identified in the pathogenesis of hepatic steatosis in children. However, NAFLD is the leading cause of hepatic steatosis in pediatric patients with increasing prevalence (15). The other less common factors of hepatic steatosis are nutritional causes (starvation, malnutrition), intoxications (carbon tetrachloride, organic phosphates, organic solvents, alcohol), drugs (glucocorticoids, estrogens, tetracyclines, methotrexate), metabolic disorders, hepatitis C infection and total parenteral nutrition. NAFLD in pediatric population is a progressive disease and 6% of the subjects will develop cirrhosis and end-stage liver disease (16). Therefore, it is important to monitor these patients (Fig. 2).

IMAGING PATTERNS

Hepatic steatosis can be seen in different patterns and being aware of these patterns is important for diagnosis. These include diffuse, focal, perilesional, periportal-perivascular, subcapsular, lobar and multinodular hepatic steatosis (17-20).

Focal Hepatic Steatosis

This form of hepatic steatosis occurs mostly as a result of aberrant hepatopetal venous flow due to presence of veins of Sappey, pancreaticoduodenal, aberrant right and left gastric

veins, which are known as third inflow (21). It is generally seen as a geographic area within the characteristic locations; gallbladder fossa, subcapsular region, adjacent to the portal vein or falciform ligament (22-24) (Fig. 3). Focal steatosis can also be detected as a nodular or mass like lesion, and fat content may not be diagnosed by CT based on Hounsfield units. In such patients, invisible fat on CT can be diagnosed by MRI (25). Also, typical location, absence of mass effect and presence of normal vascular structures traversing through the lesion is helpful in differentiating focal hepatic steatosis from other lesions. MR can be used for ruling out metastasis in cancer patients, who develop new areas of focal fat after chemotherapy. On MRI characteristic findings are isointesity on in phase images and signal drop on out of phase T1 weighted images, no diffusion restriction and isointensity on hepatobiliary phase images. Hypersteatosis is defined as focal more fatty area in diffuse steatosis and can mimic a metastasis in cancer patients (26) (Fig. 4). Also intravoxel or microscopic fat similar to focal steatosis can be present in regenerative nodule, hepatic adenoma, hepatocellular carcinoma and rarely in focal nodular hyperplasia (26).

Diffuse Hepatic Steatosis

Diffuse hepatic steatosis is the most common form of hepatic steatosis in which there is a homogeneously fatty appearance in the liver. This form can be seen in all of the etiologic causes of hepatic steatosis. Despite this homogeneous appearance on selected imaging modality, there can be small differences across the liver in quantitative analyses that will be mentioned in the next section. Also diffuse heterogeneous form can be seen and MR can be used for problem solving (Fig.5).

Perilesional, Periportal and Perivascular Hepatic Steatosis

Perilesional fat can be seen in patients with insulinoma due to local insulin effect around liver metastases (27). Fat accumulation can occur in the periportal or perivascular (around hepatic veins) areas, which surrounds portal tracts or hepatic veins with a relative fat sparing in the remainder of the liver (Fig. 5). It was shown that alcoholic cirrhosis, alcohol consumption and oral corticosteroid therapy may induce periportal-perivascular hepatic steatosis (28). This entity should be differentiated from other perivascular pathologies such as edema, hemorrhage, extramedullary hematopoiesis, fibrosis, perfusion abnormalities and neoplasia like neurofibroma and lymphoma that has a similar appearance (29, 30).

Subcapsular Hepatic Steatosis

Subcapsular fatty infiltration is commonly seen in patients who received intraperitoneal insulin within their peritoneal dialysate (31). High concentration of insulin causes local fat accumulation in the subcapsular zone. This form can be nodular in shape or involves subcapsular region like a rind. This form of hepatic steatosis can also be idiopathic.

Multinodular Hepatic Steatosis

Hepatic steatosis can be detected as multiple nodular or ovoid fat foci throughout the liver (32). This form is more frequently seen in cancer patients after chemotherapy, either as new lesions or at the location of metastatic lesions most likely due to fatty necrosis (Fig. 5). These foci may mimic multiple metastases, which is extremely problematic in patients with known malignancy. The other pathologies that have similar appearances are lymphoma, sarcoidosis, abscesses, candidiasis and biliary hamartomas. MRI should be used in such patients for differential diagnosis before biopsy.

Lobar Hepatic Steatosis

Lobar fat accumulation is a rare entity that originates from occlusion of right or left portal vein. The reason is thought to be decreased nutrient supply to one lobe that results in fat deposition differences between two lobes (33). Diagnosis of lobar hepatic steatosis can be difficult on US or CT imaging. However, signal drop on out-of-phase images relative to in-phase-images on the effected lobe on MRI is diagnostic (Fig. 6)

MIMICKERS OF STEATOSIS

Radiotherapy

Radiation-induced liver disease (radiation hepatitis) is a complication of radiotherapy and characterized with anicteric ascites, hepatomegaly and elevated liver enzymes within 2-8 weeks after radiotherapy. Irradiated liver parenchyma can appear hypodense at unenhanced CT and hypodense or hyperdense on enhanced CT (34). On MRI, it is detected as hypointense area on T1 and hyperintense on T2 images due to edema. The borders of this area are straight with no anatomic congruity. Findings usually regress in 4-6 months and irradiated area gradually shrinks with a compensatory hypertrophy in the remaining of the liver (Fig. 6).

Metastasis

Liver metastasis generally appears hypodense on CT, which may mimic hepatic steatosis foci as mentioned in the previous section (Fig. 6). Furthermore, some metastasis contains fat as they originate from fat-containing primary tumors such as teratoma, liposarcoma, Wilms' tumor and renal cell carcinoma that should be kept in mind in oncology

patients (35). Metastasis in a diffusely fatty liver, which is commonly seen in patients receiving chemotherapy, may not be easily detected on US and CT. In such patients MRI should be preferred for follow up.

Fibrosis

Confluent hepatic fibrosis is seen as a wedge-shaped area with capsular retraction and usually involves segment 4, anterior segment of right lobe or both in cirrhotic patients (36, 37). It is detected as hypodense area on unenhanced CT and becomes isodense or slightly hypodense on contrast-enhanced CT. These areas can enhance on delayed phase images on CT and MRI.

Perfusion

Liver has dual blood supply through the hepatic artery and portal vein. Despite adaptation mechanisms, decreased flow in one of them may lead to perfusion changes in the liver (38). In case of a portal venous compromise such as thrombosis or compression, perfusion differences causing attenuation differences are detected. The corresponding parenchyma, which can be lobar or focal according to the affected portal vein segment, appears as a hypoattenuating area on arterial phase images. This area can also be detected on unenhanced CT images if it has a long duration. Similar findings can be observed in hepatic venous occlusions or arterioportal shunts as portal vein undertakes the drainage task. Occlusion of hepatic artery alone does not create a meaningful perfusion difference. However, a hypoattenuating area can be identified near a hypervascular tumor due to “steal phenomenon”. In all perfusion abnormalities, dynamic contrast enhanced CT scans demonstrate phase depended attenuation differences in the liver and support the diagnosis (Fig. 6).

QUANTIFICATION OF STEATOSIS

Quantification of hepatic steatosis is an important issue as it gives information about severity of the disease. The main way to quantify hepatic steatosis is liver biopsy. However, there are potential drawbacks of liver biopsy and it is not feasible to evaluate patients with liver biopsy in every follow-up period. Hence, imaging modalities are commonly used for this purpose.

Ultrasound

Ultrasound is an initial screening tool for hepatic steatosis as being inexpensive and widely available. Hepatic steatosis is detected as increased echogenicity due to increased parenchymal reflectivity on US imaging. Normal liver echogenicity should be equal or slightly more than kidney or spleen parenchyma. Mild hepatic steatosis refers to increased echogenicity and increased discrepancy of echo amplitude between liver and kidney or spleen. Moderate hepatic steatosis can be identified with loss of echoes from the walls of the portal system and severe hepatic steatosis with posterior attenuation. This technique is highly depended on the examiner and does not provide quantitative information that may be reproducible. Besides, reported sensitivity and specificity values of US to detect hepatic steatosis are variable (39-41). Several studies investigated the accuracy of some advanced US techniques for quantification of hepatic steatosis (42-47). Despite reported accuracy values, these techniques have limited clinical use for quantification of hepatic steatosis as being complex or based on noncommercial software. Son et al. recently described the use of acoustic structure quantification (ASQ) method which is used for evaluation of diffuse liver diseases in hepatic steatosis assessment (48 and they observed that focal disturbance ratio

measured with ASQ has a strong correlation with hepatic fat fraction measured with MR spectroscopy in this pilot study.

Computed Tomography

Hepatic steatosis leads to reduction of HU value on computed tomography (CT). It is shown that the degree of hepatic steatosis is associated with degree of decrease in attenuation values (49,50). There are two main methods in estimation of hepatic steatosis with CT; hepatic measurement only and normalization of hepatic attenuation with splenic attenuation. In the first one, hepatic attenuation value can be obtained by placing one or more round of interests (ROIs) in the interested liver parenchyma. In the second one, calculation of spleen-to-liver attenuation ratio or difference between liver and spleen attenuation values can be used for estimation of hepatic steatosis degree.

Expected attenuation value of healthy liver is about 50-57 HU and 8-10 HU higher than the attenuation of spleen (51). Park et al. investigated diagnostic accuracy of hepatic attenuation value, liver-to-spleen attenuation ratio and the difference of liver and spleen attenuation value for the diagnosis of macrovesicular steatosis of 30% or higher on unenhanced CT images (52). They observed the highest specificity (100%) for 42 HU, 0.8 and -9 HU, respectively with no diagnostic superiority among them. A recent study which used liver-to-spleen attenuation ratio showed that a ratio of 0.9 discriminated 30% or more hepatic steatosis with a sensitivity of 79% and a specificity of 97% (53). Kodama et al evaluated hepatic measurement only and comparison of liver attenuation with spleen on both unenhanced and portal phase contrast-enhanced CT images (54). They found that association of all measurements with pathologic fat content is statistically significant. However, hepatic measurement only was observed as the best for prediction of pathologic fat content and a

value of 40 HU is predictable for 30% hepatic steatosis. Dual-energy CT is promising for the evaluation of hepatic steatosis which should be verified with further clinical studies (55,56). Despite satisfactory sensitivity and specificity values observed in evaluation of hepatic steatosis with CT, radiation exposure limits the usage in children and follow-up evaluation. Besides, it was shown that attenuation values vary with manufacturer and generation of the scanner which decreases the reliability of CT in quantification of hepatic steatosis (57).

MRI

MRI is commonly used in the evaluation of hepatic steatosis as being a noninvasive, nonhazardous and cross sectional imaging technique. The principle of MRI to detect and quantify fat mainly depends on chemical shift effect which can be defined as the difference of resonance frequencies between hydrogen protons bound to triglycerides and water. This difference can directly be seen on the spectra in magnetic resonance spectroscopy (MRS) or can be calculated with different MRI techniques.

MR Spectroscopy

MR spectroscopy (MRS) displays molecular composition of the interested tissue as resonance peaks at different locations on the spectra. On MRS spectra of the liver, there are two main peaks; water positioned at 4.7 ppm and fat positioned at 1.3 ppm. There are also other identifiable small fat peaks at various locations on the spectra. The signal intensities of these peaks can be quantified by spectral tracing of the peaks and fat content can be calculated by giving the ratio of signal intensities of fat peaks to the sum of fat and water peaks. MRS of the liver can be successfully performed in a single acquisition with single breath-hold. Single-voxel spectroscopy (SVS) is commonly preferred for fat quantification of the liver which can be acquired with stimulated echo acquisition mode (STEAM) or a point-resolved spectroscopy (PRESS) sequence. STEAM is accepted as a better sequence for fat

quantification as it is less susceptible to J-coupling effects despite a higher signal-to-noise ratio observed in PRESS sequence (58). In SVS, data is collected from a single voxel which is placed on the interested liver parenchyma avoiding vessels, bile ducts and surrounding adipose tissue.

The first study by Longo et al. showed good correlation between MRS and histology determined hepatic steatosis (59) and following studies supported this finding (60,61). High intra-individual reproducibility was also observed in repeated measurements in the MRS (62-64). Therefore, MRS was accepted as a reference imaging method for assessment of hepatic steatosis. However, MRS demonstrates fat fraction of a limited portion of the liver, is not available on all clinical scanners and requires post-processing software and specific analyses by a physicist which limits the usage of the technique as a daily routine. These factors accelerated development of other MRI techniques in the use of quantification of hepatic steatosis.

MRI techniques

Hepatic steatosis can be detected as increased hepatic signal intensity on conventional T1 weighted MR images. However, quantification of hepatic fat is feasible with specific MRI techniques including chemical-shift imaging (CSI) and fat-suppressed imaging approaches. Fat-suppressed imaging techniques use the effect of fat-suppression pulses to observe a decrease in hepatic steatosis and by the way detect fat containing liver. CSI separates the signals into water and fat by using a similar principle with MRS; the chemical shift-induced signal interference between the protons in fat and water.Net magnetization vectors of protons of fat (methylene) and water are positioned in in phase (IP) (water + fat) and opposed phase (OP) (water - fat) depending on the chosen echo time (TE). By the way, fat fraction of the interested tissue can be calculated by measuring the signal intensities on IP and OP images.

This approach was first introduced by Dixon et al. (65) and has been improved in recent years. Despite a wide clinical usage of the basic CSI technique, it is prone to biases from T1 and T2* relaxation that may lead to inaccurate fat quantification. Further techniques aimed to minimize these factors by using low flip angle and multiple echo acquisition, respectively. Recently, Reeder et al defined a complex CSI based technique called IDEAL (iterative decomposition of water and fat with echo asymmetry and least-squares estimation) which is capable to measure proton density fat fraction (PDFF) of the liver by separating the signals from water and fat (66). Clinical studies using this technique showed a close correlation between histology determined steatosis and MRI-PDFF determined steatosis with high accuracy rates and currently this method (IDEAL-IQ, LiverQuant, mdixonQuant) is commercially available by all vendors under different names (67-69) (Fig. 7). Moreover, following studies demonstrated that the technique can also be used for quantification of longitudinal changes in hepatic fat content in NAFLD patients (70,71) (Fig. 8).

The studies comparing MRI-PDFF with MRS determined hepatic steatosis demonstrated an excellent correlation (72,73). A recent study observed a good correlation among MRI and MRS determined hepatic steatosis in comparison with histology determined hepatic steatosis with no superiority among them (74). However, it was shown that there can be significant fat distribution differences among different regions of the liver which is a limitation for MRS (75). MRI-PDFF allows assessment of the whole liver in less than 20 seconds without a specialized physicist to calculate fat fraction and therefore becomes a better approach for quantification of hepatic steatosis. Moreover, iron content of the liver can be determined by T2* maps obtained simultaneously and therefore opposing effects of fat and iron can be solved by using the same multiecho gradient echo sequence for PDFF calculation (76) (Fig. 9). Recently, feasibility of fatty acid maps has also been reported, which may enable detailed analysis of hepatic steatosis (77).

NAFLD can progress into steatohepatitis (NASH), which can end up with cirrhosis. The pathological findings of NASH include inflammation and various degrees of fibrosis besides steatosis. Therefore, new imaging techniques aim to demonstrate these associated features. MR elastography and functional evaluation with Gd-EOB-DTPA are becoming important for monitoring this process (78-81). It was shown that hepatobiliary-phase enhancement ratio showed significant association with steatohepatitis and fibrosis stage in patients with NAFLD (Fig.10) (78). The accuracy of magnetic resonance elastography for staging liver fibrosis was also shown in different studies (79-81). Hepatocellular carcinoma can also develop in patients with NAFLD which is usually a large tumor with necrotic center (Fig.11) (82,83). It is important to identify an HCC in a fatty liver as up to 25% of the patient with NASH can progress to HCC (84). Moreover, cardiovascular disease associated with NAFLD can be assessed by coronary ct angiography and measuring liver density on noncontrast CT slices obtained for calcium scoring (85).

CONCLUSION

There are various etiologic causes and imaging patterns of hepatic steatosis, which are important for radiologic diagnosis. In cancer patients some forms of steatosis can mimic metastasis, therefore in patients with equivocal findings on ultrasonography and CT, MRI should be performed for differential diagnosis. Quantification of hepatic steatosis beyond detection is feasible and proton density fat fraction is becoming a biomarker for follow-up of NAFLD patients. In the future, fatty acid maps may allow more detailed analysis of steatosis.

REFERENCES

1. Angulo P. Obesity and nonalcoholic fatty liver disease. Nutr Rev 2007;65:57-63.
2. Ratziu V,Charlotte F, Heurtier A, et al. Sampling variability of liver biopsy in nonalcoholic fatty liver disease. Gastroenterology 2005;128:1898-906.
3. Janiec DJ, Jacobson ER, Freeth A, et al. Histologic variation of grade and stage of non-alcoholic fatty liver disease in liver biopsies. Obes Surg 2005;15:497-501.
4. Browning JD, Szczepaniak LS, Dobbins R et al. Prevalence of hepatic steatosis in an urban population in the United States: impact of ethnicity. Hepatology 2004;40:1387-1395.
5. Targher G. Non-alcoholic fatty liver disease, the metabolic syndrome and the risk of cardiovascular disease: the plot thickens. Diabet Med 2007;24:1-6.
6. de Alwis NM, Day CP. Non-alcoholic fatty liver disease: the mist gradually clears. J Hepatol 2008; 48 Suppl 1:104-112
7. Byrne CD, Targher G. NAFLD: a multisystem disease. J Hepatol 2015; 62:47-64.
8. Teli MR, Day CP, Burt AD et al. Determinants of progression to cirrhosis or fibrosis in pure alcoholic fatty liver. Lancet 1995;346:987–990.
9. Mandayam S, Jamal MM, Morgan TR. Epidemiology of alcoholic liver disease. Semin Liver Dis 2004; 24: 217-232.
10. Bellentani S, Saccoccio G, Costa G et al. Drinking habits as cofactors of risk for alcohol induced liver damage. The Dionysos Study Group. Gut 1997; 41: 845-850.
11. Negro F. Mechanisms and significance of liver steatosis in hepatitis C virus infection.World J Gastroenterol. 2006 ;12(42):6756-65.
12. Asselah T, Rubbia-Brandt L, Marcellin P, Negro F. Steatosis in chronic hepatitis C: why does it really matter? Gut. 2006 ;55(1):123-30.

13. González-Reimers E, Quintero-Platt G, Rodríguez-Gaspar M et al. Liver steatosis in hepatitis C patients. World J Hepatol. 2015;7:1337-46.

14. Amacher DE, Chalasani N. Drug-induced hepatic steatosis. Semin Liver Dis. 2014 ;34(2):205-14.

15. Pardee PE, Lavine E, Schwimmer JB. Diagnosis and treatment of pediatric nonalcoholic steatohepatitis and the implications for bariatric surgery. Semin Pediatr. Surg 2009;18:144-51.

16. Feldstein AE, Charatcharoenwitthaya P, Treeprasertsuk S et al. The natural history of nonalcoholic fatty liver disease in children: a follow-up study for up to 20 years. Gut 2009; 58: 1538-1544.

17. Karcaaltincaba M, Akhan O. Imaging of hepatic steatosis and fatty sparing.Eur J Radiol. 2007 ;61(1):33-43.

18. Vilgrain V, Ronot M, Abdel-Rehim M et al. Hepatic steatosis: a major trap in liver imaging. Diagn Interv Imaging. 2013;94:713-27

19. Özcan HN, Oğuz B, Haliloğlu M et al. Imaging patterns of fatty liver in pediatric patients. Diagn Interv Radiol. 2015;21:355-60.

20. Dioguardi Burgio M, Bruno O, Agnello F et al. The cheating liver: imaging of focal steatosis and fatty sparing. Expert Rev Gastroenterol Hepatol. 2016 Apr 6:1-8. [Epub ahead of print]

21. Unal E, Ozmen MN, Akata D, Karcaaltincaba M. Imaging of aberrant left gastric vein and associated pseudolesions of segments II and III of the liver and mimickers. Diagn Interv Radiol. 2015;21:105-10.

22. Yoshikawa J, Matsui O, Takashima T et al. Focal fatty change of the liver adjacent to the falciform ligament: CT and sonographic findings in five surgically confirmed cases.AJR Am J Roentgenol. 1987 ;149(3):491-4.

23. Matsui O, Kadoya M, Takahashi S et al. Focal sparing of segment IV in fatty livers shown by sonography and CT: correlation with aberrant gastric venous drainage. AJR Am J Roentgenol. 1995;164(5) :1137-40.

24. Valls C, Iannacconne R, Alba E et al. Fat in the liver: diagnosis and characterization. Eur Radiol. 2006;16(10):2292-308.

25. Ünal E, Karaosmanoğlu AD, Akata D et al. Invisible fat on CT: making it visible by MRI. Diagn Interv Radiol. 2016;22:133-40.

26. Basaran C, Karcaaltincaba M, Akata D et al. Fat-containing lesions of the liver: cross-sectional imaging findings with emphasis on MRI. AJR Am J Roentgenol. 2005;184: 1103-10.

27. Sohn J, Siegelman E, Osiason A. Unusual patterns of hepatic steatosis caused by the local effect of insulin revealed on chemical shift MR imaging. Am J Roentgenol 2001;176:471–4.

28. Hamer OW, Aguirre DA, Casola G, Sirlin CB. Imaging features of perivascular fatty infiltration of the liver: initial observations. Radiology. 2005;237:159-69.

29. Lawson TL, Thorsen MK, Erickson SJ et al. Periportal halo: a CT sign of liver disease. Abdom Imaging 1993;18:42–46.

30. Karcaaltincaba M, Haliloglu M, Akpinar E et al. Multidetector CT and MRI findings in periportal space pathologies. Eur J Radiol. 2007;61:3-10.

31. Khalili K, Lan FP, Hanbidge AE et al. Hepatic subcapsular steatosis in response to intraperitoneal insulin delivery: CT findings and prevalence. AJR Am J Roentgenol 2003;180(6):1601–1604.
32. Prasad SR, Wang H, Rosas H et al. Fat-containing lesions of the liver: radiologic pathologic correlation. Radiographics 2005;25:321–331.
33. Karçaaltincaba M, Sirlin CB. CT and MRI of diffuse lobar involvement pattern in liver pathology. Diagn Interv Radiol. 2011;17:334-42.
34. Unger EC, Lee JK, Weyman PJ. CT and MR imaging of radiation hepatitis. J Comput Assist Tomogr. 1987;11:264-8.
35. Bartolozzi C, Cioni D, Donati F, Lencioni R. Focal liver lesions: MR imaging–pathologic correlation. Eur Radiol 2001;11:1374–1388.
36. Ohtomo K, Baron RL, Dodd III GD et al. Confluent hepatic fibrosis in advanced cirrhosis: evaluation with MR imaging. Radiology 1993;189:871–4.
37. Peterson MS1, Baron RL, Dodd GD 3rd et al. Hepatic parenchymal perfusion defects detected with CTAP: imaging-pathologic correlation. Radiology. 1992;185(1):149-55
38. Desser TS. Semin Ultrasound CT MR. Understanding transient hepatic attenuation differences. 2009;30(5):408-17.
39. Foster KJ, Dewbury KC, Griffith AH, Wright R. The accuracy of ultrasound in the detection of fatty infiltration of the liver. Br J Radiol 1980;53:440–442.
40. Debongnie JC, Pauls C, Fievez M, Wibin E. Prospective evaluation of the diagnostic accuracy of liver ultrasonography. Gut 1981;22:130–135.
41. Graif M, Yanuka M, Baraz M et al. Quantitative estimation of attenuation in ultrasound video images: correlation with histology in diffuse liver disease. Invest Radiol 2000;35:319–324.

42. Kim SH, Lee JM, Kim JH, et al. Appropriateness of a donor liver with respect to macrosteatosis: application of artificial neural networks to US images—initial experience.Radiology 2005;234(3):793–803.

43. Strauss S, Gavish E, Gottlieb P, Katsnelson L. Interobserver and intraobserver variability in the sonographic assessment of fatty liver. AJR Am J Roentgenol 2007; 189(6):W320–W323.

44. Edens MA, van Ooijen PM, Post WJ, et al. Ultrasonography to quantify hepatic fat content:validation by 1H magnetic resonance spectroscopy. Obesity (Silver Spring) 2009; 17:2239–2244.

45. Mancini M, Prinster A, Annuzzi G, et al. Sonographic hepatic-renal ratio as indicatorof hepatic steatosis: comparison with (1)H magnetic resonance spectroscopy. Metabolism 2009;58(12):1724–1730.

46. Acharya UR, Sree SV, Ribeiro R, et al. Data mining framework for fatty liver diseaseclassification in ultrasound: a hybrid feature extraction paradigm. Med Phys 2012;39(7):4255–4264.

47. Mihăilescu DM, Gui V, Toma CI et al. Computer aided diagnosis method for steatosis rating in ultrasound images using random forests. Med Ultrason 2013;15(3): 184–190.

48. Son JY, Lee JY, Yi NJ et al. Hepatic Steatosis: Assessment with Acoustic Structure Quantification of US Imaging. Radiology. 2016;278(1):257-64.

49. Ducommun JC, Goldberg HI, Korobkin M et al The relation of liver fat to computed tomography numbers: a preliminary experimentalstudy in rabbits. Radiology 1979;130:511–513.

50. Ricci C, Longo R, Gioulis E, et al. Noninvasive in vivo quantitative assessment of fat content in human liver. J Hepatol 1997;27:108–113.

51. Piekarski J, Goldberg HI, Royal SA et al. Difference between liver and spleen CT numbers in the normal adult: its usefulness in predicting the presence of diffuse liver disease. Radiology 1980;137:727–729.

52. Park SH, Kim PN, Kim KW et al. Macrovesicular hepatic steatosis in living liver donors: use of CT for quantitative and qualitative assessment. Radiology 2006;239:105–112.

53. Rogier J, Roullet S, Cornélis F et al. Noninvasive assessment of macrovesicular liver steatosis in cadaveric donors based on computed tomography liver-to-spleen attenuation ratio. Liver Transpl. 2015;21(5): 690-5.

54. Kodama Y, Ng CS, Wu TT et al. Comparison of CT methods for determining the fat content of the liver. Am J Roentgenol 2007;188:1307–1312.

55. Karçaaltıncaba M, Aktaş A. Dual-energy CT revisited with multidetector CT: review of principles and clinical applications. Diagn Interv Radiol. 2011;17(3):181-94

56. Artz NS, Hines CD, Brunner ST et al. Quantification of hepatic steatosis with dual-energy computed tomography: comparison with tissue reference standards and quantitative magnetic resonance imaging in the ob/ob mouse. Invest Radiol. 2012;47(10):603-10.

57. Birnbaum BA, Hindman N, Lee J, Babb JS. Multi-detector row CT attenuation measurements: assessment of intra- and interscanner variability with an anthropomorphic body CT phantom. Radiology 2007;242:109–119.

58. Hamilton G, Middleton MS, Bydder M et al. Effect of PRESS and STEAM sequences on magnetic resonance spectroscopic liver fat quantification. J Magn Reson Imaging 2009;30: 145-152.

59. Longo R, Ricci C, Masutti F et al. Fatty infiltration of the liver. Quantification by 1H localized magnetic resonance spectroscopy and comparison with computed tomography. Invest Radiol 1993;28:297–302.

60. Thomsen C, Becker U, Winkler K et al. Quantification of liver fat using magnetic resonance spectroscopy. Magn Reson Imaging 1994;12:487–495.

61. Szczepaniak LS, Babcock EE, Schick F et al. Measurement of intracellular triglyceride stores by H spectroscopy: validation in vivo. Am J Physiol 1999;276: E977–E989.

62. Cowin GJ, Jonsson JR, Bauer JD et al. Magnetic resonance imaging and spectroscopy for monitoring liver steatosis. J Magn Reson Imaging 2008; 28: 937-945

63. Machann J, Thamer C, Schnoedt B et al. Hepatic lipid accumulation in healthy subjects: a comparative study using spectral fat-selective MRI and volume-localized 1H-MR spectroscopy. Magn Reson Med 2006; 55: 913-917

64. Szczepaniak LS, Nurenberg P, Leonard D et al. Magnetic resonance spectroscopy to measure hepatic triglyceride content: prevalence of hepatic steatosis in the general population. Am J Physiol Endocrinol Metab 2005; 288: E462-E468

65. Dixon WT. Simple proton spectroscopic imaging. Radiology 1984;153:189–194.

66. Reeder SB, Robson PM, Yu H, et al. Quantification of hepatic steatosis with MRI: the effects of accurate fat spectral modeling. J Magn Reson Imaging 2009;29(6):1332–1339.

67. Permutt Z, Le TA, Peterson MR et al. Correlation between liver histology and novel magnetic resonance imaging in adult patients with non-alcoholic fatty liver disease – MRI accurately quantifies hepatic steatosis in NAFLD. Aliment Pharmacol Ther 2012;36:22-29.

68. Tang A, Tan J, Sun M et al. Nonalcoholic fatty liver disease: MR imaging of liver proton density fat fraction to assess hepatic steatosis. Radiology 2013;267:422-431.

69. Idilman IS, Aniktar H, Idilman R et al. Hepatic steatosis: quantification by proton density fat fraction with MR imaging versus liver biopsy. Radiology 2013;267:767-775.

70. Noureddin M, Lam J, Peterson MR et al. Longitudinal comparison between MRI, MRS and histology-determined steatosis in NAFLD patients at two-time points in a randomized trial. Hepatology 2013;58:1930–40.

71. Idilman IS, Keskin O, Elhan AH et al. Impact of sequential proton density fat fraction for quantification of hepatic steatosis in nonalcoholic fatty liver disease. Scand J Gastroenterol, 2014;49:617-624.

72. Kim H, Taksali SE, Dufour S, et al. A comparative MR study of hepatic fat quantification using single-voxel proton spectroscopy, two-point Dixon and three-point IDEAL. Magn Reson Med 2008;59:521-527.

73. Meisamy S, Hines CD, Hamilton G, et al. Quantification of hepatic steatosis with T1-independent, T2-corrected MR imaging with spectral modeling of fat: blinded comparison with MR spectroscopy. Radiology 2011;256:767-775.

74. Idilman IS, Keskin O, Celik A et al. A comparison of liver fat content as determined by magnetic resonance imaging-proton density fat fraction and MRS versus liver histology in non-alcoholic fatty liver disease. Acta Radiol, 2016;57:271-278.

75. Cowin GJ, Jonsson JR, Bauer JD et al.. Magnetic resonance imaging and spectroscopy for monitoring liver steatosis. J Magn Reson Imaging 2008;28:937–945.

76. İdilman İS, Akata D, Özmen MN, Karçaaltıncaba M. Different forms of iron accumulation in the liver on MRI. Diagn Interv Radiol. 2016;22(1):22-8.

77. Leporq B, Lambert SA, Ronot M et al. Quantification of the triglyceride fatty acid composition with 3.0 T MRI. NMR Biomed. 2014 Oct;27(10):1211-21.

78. Wu Z, Matsui O, Kitao A et al. Usefulness of Gd-EOB-DTPA-enhanced MR imaging in the evaluation of simple steatosis and nonalcoholic steatohepatitis. J Magn Reson Imaging. 2013 May;37(5):1137-43.

79. Loomba R, Cui J, Wolfson T et al. Novel 3D Magnetic Resonance Elastography for the Noninvasive Diagnosis of Advanced Fibrosis in NAFLD: A Prospective Study.Am J Gastroenterol. 2016 Mar 22. doi: 10.1038/ajg.2016.65. [Epub ahead of print]

80. Cui J, Heba E, Hernandez C et al. Magnetic resonance elastography is superior to acoustic radiation force impulse for the Diagnosis of fibrosis in patients with biopsy-proven nonalcoholic fatty liver disease: A prospective study. Hepatology. 2016 Feb;63(2):453-61.

81. Singh S, Venkatesh SK, Loomba R et al. Magnetic resonance elastography for staging liver fibrosis in non-alcoholic fatty liver disease: a diagnostic accuracy systematic review and individual participant data pooled analysis. Eur Radiol. 2016 May;26(5):1431-40.

82. Brancatelli G, Federle MP, Grazioli L, Carr BI. Hepatocellular carcinoma in noncirrhotic liver: CT, clinical, and pathologic findings in 39 U.S. residents. Radiology. 2002 Jan;222(1):89-94.

83. Iannaccone R, Piacentini F, Murakami T et al. Hepatocellular carcinoma in patients with nonalcoholic fatty liver disease: helical CT and MR imaging findings with clinical-pathologic comparison. Radiology. 2007 May;243(2):422-30.

84. Charrez B, Qiao L, Hebbard L. Hepatocellular carcinoma and non-alcoholic steatohepatitis: The state of play. World J Gastroenterol. 2016 Feb 28;22(8):2494-502.

85. Idilman IS, Akata D, Hazirolan T et al. Nonalcoholic fatty liver disease is associated with significant coronary artery disease in type 2 diabetic patients: a computed tomography angiography study. J Diabetes. 2015;7(2):279-86.

FIGURE LEGENDS

Figure 1: 55 year old man after FOLFOX chemotherapy for colon cancer with elevated liver enzymes. PDFF map shows heterogeneous steatosis ranging from 12% to 29%.

Figure 2: An 8-year-old boy with focal hyperechogenic areas in segment 4 on US (a). In (b) and out of phase images (c) demonstrate signal drop which confirms heterogeneous steatosis (arrows).

Figure 3: A focal hyperechogenic (arrow) area is seen in segment 4 on US evaluation (a). The same area (arrow) is seen hypodense at CT (b). The diagnosis of focal hepatic steatosis is confirmed with in (c) and out of phase (arrow) MR images (d).

Figure 4: A 50 year old women with breast cancer. Hypersteatosis is seen in segment 4 as a focal hypodense area (arrow) within a background of diffuse fatty liver on CT (a). MRI-PDFF (b) demonstrates a higher fat content at that area (38%) compared to the rest of the liver (27%).

Figure 5: Various imaging patterns on in (a, c, e, g) and out of phase (b, d, f, h) MR images are seen in different patients. Heterogeneous hepatic steatosis (a, b), perivascular hepatic steatosis (c, d), perilesional (arrows) hepatic steatosis in a patient with insulinoma metastasis

(e, f) and multinodular hepatic steatosis (arrows) developed after chemotherapy (g, h) are seen as signal drop on out of phase images (b, d, f, h) compared to in phase images (a, c, e, g).

Figure 6: CT findings of lobar steatosis of left lobe confirmed by signal drop on out of phase MRI (a) and mimickers. Hypodense appearance in left lobe was confirmed as metastasis in a patient with colon cancer by MR and biopsy (b). Left lobe appears hypodense on arterial phase, which is normal and hyperdensity of right lobe is due to thrombus in right portal vein associated with hyperperfusion of right lobe (c). Left lobe and part of segment 5 appears hypodense due to radiotherapy after gastrectomy for stomach cancer (d).

Figure 7: Proton density fat fraction MR images of patients with 10% (mild) (a), 25% (moderate) (b), and 50% (severe) (c) hepatic steatosis.

Figure 8: Baseline (a) and 8 month follow up MRI-PDFF images (b) of a 50 years old male patient with NAFLD demonstrate improvement in hepatic fat content from 22% to 10%.

Figure 9: MRI-PDFF (a) and T2* color maps (b) obtained by the same sequence (mdixon-quant) demonstrate the feasibility of measurement of both fat fraction and T2* value of the liver. The fat fraction (38%) and T2* measurements (13ms) of the liver is consistent with both severe hepatic fat and mild iron accumulation.

Figure.10. Axial MRI at hepatobiliary phase after Gd-EOB-DTPA administration shows decreased enhancement (relative enhancement ratio of 0.7) consistent with decreased function (consistent with steatohepatitis or fibrosis) due to nonalcoholic fatty liver disease.

Figure 11: A large hepatocellular carcinoma is shown on in (a) and out of phase MR images (b) in a patient nonalcoholic fatty liver disease. Capsule, washout and nonenhancing necrotic area (arrow) can be clearly identified on post-contrast T1W image (c). Tumor was hypervascular on arterial phase image.